Asia-Pac. J. Atmos. Sci., 53(2), 207-216, 2017
DOI:10.1007/s13143-017-0027-2
pISSN 1976-7633 / eISSN 1976-7951

Development of Statistical Prediction Models for Changma Precipitation: An Ensemble Approach

Jin-Yong Kim, Kyong-Hwan Seo, Jun-Hyeok Son, and Kyung-Ja Ha

Division of Earth Environmental System, Department of Atmospheric Sciences, Pusan National University, Busan, Korea

(Manuscript received 13 October 2016; accepted 2 February 2017)

Abstract: An ensemble statistical forecast scheme with a one-month lead is developed to predict year-to-year variations of Changma rainfall over the Korean peninsula. Spring sea surface temperature (SST) anomalies over the North Atlantic, the North Pacific and the tropical Pacific Ocean have been proposed as useful predictors in a previous study. Through a forward-stepwise regression method, four additional springtime predictors are selected: the northern Indian Ocean (NIO) SST, the North Atlantic SST change (NAC), the snow cover anomaly over the Eurasian continent (EUSC), and the western North Pacific outgoing longwave radiation anomaly (WNP (OLR)). Using these, three new prediction models are developed. A simple arithmetic ensemble mean produces much improved forecast skills compared to the original prediction model of Lee and Seo (2013). Skill scores measured by temporal correlation and MSSS (mean square error skill score) are improved by about 9% and 17%, respectively. The GMSS (Gerrity skill score) and hit rate based on a tercile prediction validation scheme are also enhanced by about 19% and 13%, respectively. The reversed NIO, reversed WNP (OLR), and reversed NAC are all related to the enhancement of a cyclonic circulation anomaly to the south or southwest of the Korean peninsula, which induces southeasterly moisture flux into the peninsula and increasing Changma precipitation. The EUSC predictor induces an enhancement of the Okhotsk Sea high downstream and thus strengthening of Changma front.

Key words: Changma, East Asian summer monsoon, Changma front, statistical prediction model, ensemble forecast

1. Introduction

Changma is the major rainy season over the Korean peninsula and a subsystem of the East Asian summer monsoon (EASM) (Wang et al., 2007; Chu et al., 2012; Lee and Seo 2013). It accounts for more than 30% of the annual total rainfall in this region, making Changma one of the dominant factors that determine summertime climate and its variability over the Korean peninsula. Since Changma exerts extensive influence on agriculture, human lives, economics, etc., skillful prediction of the year-to-year variability of Changma precipitation is of great importance for preventing damages in this region.

Corresponding Author: Kyong-Hwan Seo, Division of Earth Environmental System, Department of Atmospheric Sciences, Pusan National University, Busan 46241, Korea
E-mail: khseo@pusan.ac.kr

Although state-of-the-art climate models have improved significantly in recent decades and can be used as practical tools for seasonal prediction, their prediction skills for Changma precipitation remain unsatisfactory (Wu et al., 2009; Lee et al., 2011; Seo et al., 2015). In particular, prediction of precipitation during the Changma period is more difficult than that of the Indian summer monsoon, western North Pacific (WNP) summer monsoon, and EASM. The primary reason for this difficulty is that the Changma system is affected by a variety of air masses, including tropical monsoon air, cold dry air from the continent of Asia, North Pacific subtropical high (NPSH) air, cold moist air over the Okhotsk Sea, and polar air (Seo et al., 2011). In addition, mountainous terrain and the three seas that surround the Korean peninsula complicate predictions of Changma precipitation variations.

Several studies have suggested that statistical prediction models using multivariate linear regressions are useful for the prediction of interannual variability of the EASM and Changma rainfall (Wu et al., 2009; Lee and Seo, 2013; Kim and Seo, 2014; Yim et al., 2014; Seo et al., 2015; Yim et al., 2015; Oh and Ha, 2016). An empirical prediction model for July precipitation over northern East Asia was developed by Seo et al. (2015), in which four different predictors are selected, including sea surface temperature (SST) anomalies over the tropical central Indian Ocean, the Central Pacific Ocean, the northwestern Pacific Ocean, and the North Atlantic. More closely related to the present study, in order to predict Changma precipitation over South Korea, Lee and Seo (2013) constructed a statistical forecast model based on three different springtime SST predictors located over the North Atlantic (denoted as NA1), the North Pacific (NPC), and the Central Pacific Ocean (CNINO). A recent study of Kim and Seo (2014) tried to find additional predictors to enhance the statistical forecast skills of Changma precipitation. Since a variety of predictor forcing mechanisms located upstream and downstream of the Korean peninsula impact Changma precipitation, additional prediction equations must be constructed to enhance prediction skill. Here, we develop three additional prediction schemes using oceanic, land, and atmospheric predictors. A simple ensemble is performed, which achieves much improved forecast skills compared to the original prediction model of Lee and Seo (2013).

The remainder of this paper is structured as follows. A

description of the data and methods used is presented in section 2. Statistical forecast models are introduced and their performance is evaluated in section 3. In section 4, possible physical processes for each predictor are suggested. Section 5 shows an example of the role of the most dominant springtime predictor signals in influencing low-level circulation features and thereby Changma precipitation for the three most recent Changma years. A summary is presented in section 6.

2. Data and methods

a. Data

Changma rainfall intensity is defined as the precipitation anomaly averaged from mid-June to end of July (15 June - 29 July). The precipitation is averaged over 60 meteorological stations located in South Korea with typhoon days removed to consider large-scale dynamics. The removed typhoon days are those days when typhoons were located right over the Korea peninsula or when these were situated near the peninsula but induced rainfall over South Korea. This definition is the same as that used by previous studies (Lee and Seo, 2013; Kim and Seo, 2014).

The following daily and weekly mean datasets for the period from 1994 to 2016 are used: 1) National Oceanic and Atmospheric Administration (NOAA) Optimum Interpolation SST version 2 high resolution dataset (OISST, v2; Reynolds et al., 2007), 2) the Climate Data Record (CDR) of Northern Hemisphere (NH) Snow Cover Extent (SCE) (Robinson et al., 1993), 3) NOAA Daily Outgoing Longwave Radiation (OLR), 4) Global Precipitation Climatology Project (GPCP) precipitation (Adler et al., 2003), and 5) National Centers for Environmental Prediction/Department of Energy (NCEP-DOE) Reanalysis 2 datasets in pressure levels (Kanamitsu et al., 2002).

b. Methodology

Four multiple linear regression prediction models are constructed to forecast Changma rainfall anomalies over the Korean peninsula. For this, four predictors are found from springtime SST, OLR, and snow cover anomalies, and a forward stepwise regression method is used to select predictors and build the prediction models. All variables are normalized so that the calculated regression coefficients explicitly represent the relative weighting among predictors. To avoid overfitting and to attain stability, each prediction model is limited to having three predictors (Lee and Seo, 2013; Kim and Seo, 2014).

First, we search significant correlation areas between Changma precipitation time series and springtime data from slowly varying boundary forcing (e.g., SST and Eurasian snow cover) or atmospheric variables (e.g., OLR). Then, all significant areas are chosen as candidates for potential predictors of the prediction model.

Second, the cross-validation method with a leave-four-years-out scheme is used to prevent overfitting and to obtain the optimal regression coefficient (Blockeel and Struyf, 2002; Lee and Seo, 2013; Kim and Seo, 2014). This method produces five different sets of regression coefficients for each prediction model (i.e., for the same predictors) during the total training period from 1994 to 2011. The hindcast year 1994 was selected to avoid the effect of the recent interdecadal change. For example, precipitation patterns in the EASM and the WNP summer monsoon have been reported to experience a significant decadal change around 1993-1994 (e.g., Kwon et al., 2005). Recently, Chen and Zhou (2014) also revealed that the Pacific-Japan pattern, which is closely related to the EASM, exhibits a periodicity change from 4-5 to 2-3 years at around 1993-1994.

Finally, the correlation coefficients among potential predictors should be less than 0.3 to attain statistical independence. To avoid any potential multicollinearity, the variance inflation factor is calculated among potential predictors and only predictors with a value of less than two are included. This process is repeated until three optimal predictors are selected and have meaningful physical interpretations.

Statistical analyses were performed for forecast assessment using estimates of temporal correlation, the mean-square error skill score (MSSS), and a Gerrity skill score [or a Gandin-Murphy skill score (GMSS)]. The GMSS is similar to a hit rate estimate but with more weighting put on non-normal correct predictions (i.e., above-normal observation vs. above-normal prediction and below-normal observation vs. below-normal prediction). The MSSS ranges from −1.0 to 1.0, whereas the GMSS ranges from 0.0 to 1.0. To visualize the tercile prediction performance, a 3×3 contingency table for forecast and observation is presented (Table 3). The three categories (above normal, near-normal, and below normal years) are separated by a standard deviation of $\pm$ 0.43. The diagonal cells represent correct prediction.

3. Results

The regression patterns between Changma rainfall anomalies and springtime global and regional SST anomalies (SSTAs), OLR anomalies and Northern Hemisphere snow cover anomalies are shown in Fig. 1. All selected predictors are either persistent from March to May or show a temporal tendency from early spring to late spring. First, the three SSTA predictors selected in Lee and Seo (2013) are shown for the tropical Central Pacific, the North Pacific, and the North Atlantic (namely, CNINO, NPC, and NA1) in Fig. 1a. Additionally, SSTAs over the northern Indian Ocean (Fig. 1b) is an important predictor. The SST change in the North Atlantic (Fig. 1c), the negative OLR anomaly over the WNP during May (Fig. 1d), and west-east dipole snow cover anomalies over Eurasia during spring (Fig. 1e) are also significantly correlated with Changma precipitation.

Table 1 represents areas and periods of the seven indepen-

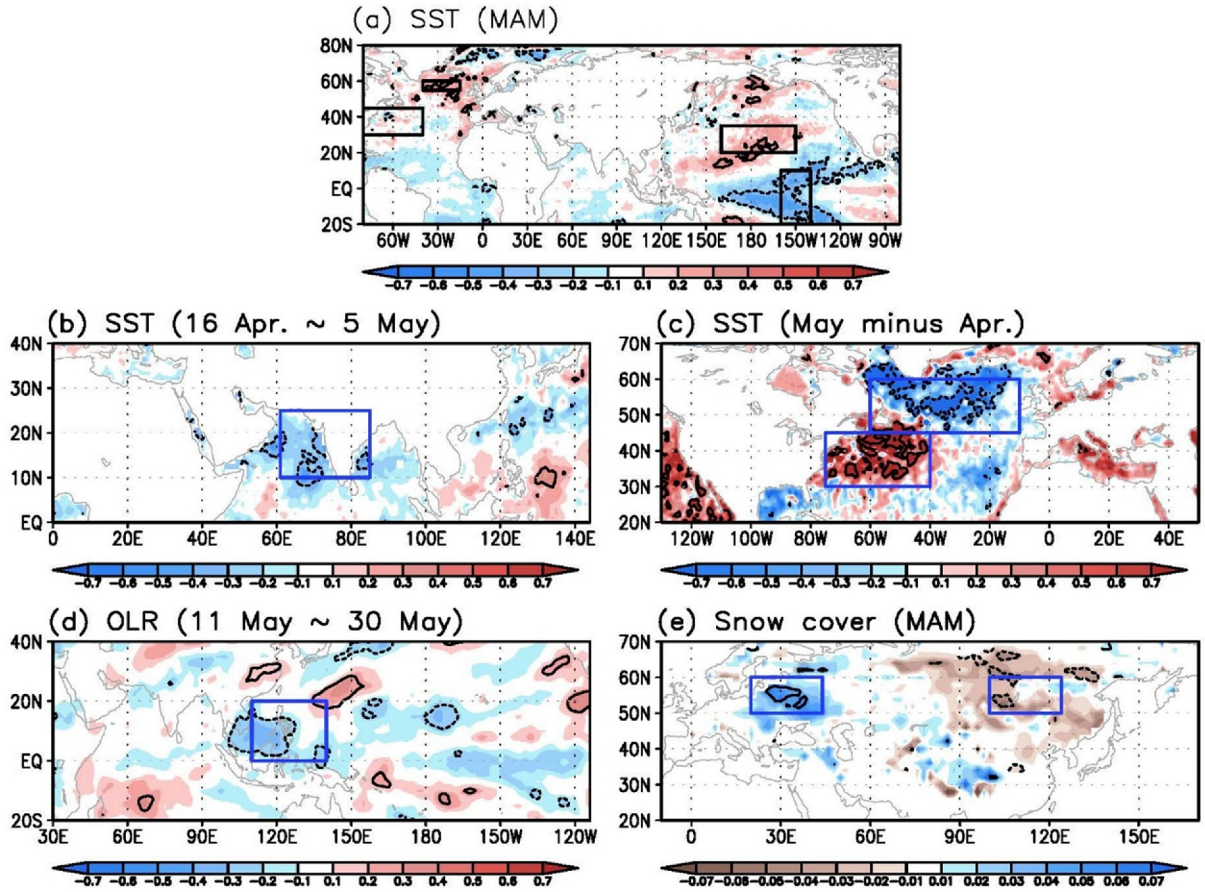

Fig. 1. The SSTAs (shading intervals of 0.1 K) for (a) March-April-May (MAM), (b) mid-April to early May, and (c) May minus April, (d) OLR anomalies (shading, intervals of 0.1 W m^{-2}) for May, and (e) snow cover anomalies (shading intervals of 0.01) for MAM (all for 1994-2011) regressed against the Changma precipitation time series. Thick black contour indicates statistically significant areas at the 90% confidence level. Black boxes in (a) represent areas of the three predictors selected in Lee and Seo (2013): North Atlantic (NA1), North Pacific (NPC) and Central Pacific NINO (CNINO). Blue boxes in (b)-(e) represent areas of the four predictors selected in this study: the northern Indian Ocean (NIO), western North Pacific (WNP(OLR)), North Atlantic change (NAC) and Eurasian snow cover (EUSC).

Table 1. List of selected predictors. Each predictor is highly correlated with the Changma precipitation time series, which is statistically significant at the 90% confidence level.

Predictors	Areas	Period
North Atlantic 1 (NA1)	[40°-15°W, 55°-60°N] - [80°-40°W, 30°-45°N]	4/6-4/25
Northern Pacific change (NPC)	160°-210° E, 20°-35° N	(4/11-4/30) - (3/22-4/10)
Central Pacific NINO (CNINO)	160°-140°W, 15°S-10°N	4/1-4/20
northern Indian Ocean (NIO)	61°-85°E, 10°-25°N	4/16-5/5
western North Pacific (WNP(OLR))	110°-140°E, 0°-20°N	5/11-5/30
North Atlantic change (NAC)	[60°-10°W, 45°-60°N] - [75°-40°W, 30°-45°N]	(5/1-5/31) - (4/1-4/30)
Eurasian snow cover (EUSC)	[20°-44°E, 50°-60°N] - [100°-124°E, 50°-60°N]	3/1-5/31

dent predictors that are significantly correlated with Changma rainfall. Domains for the predictors are shown in Fig. 2: The North Atlantic 1 (NA1), the North Atlantic change (NAC), the Eurasian snow cover (EUSC), the northern Indian Ocean (NIO), the western North Pacific (WNP (OLR)), the North Pacific change (NPC), and Central Pacific NINO (CNINO). Three of these predictors, NA1, NPC, and CNINO, are selected from a previous study (Lee and Seo, 2013). The four additional predictors, NIO, WNP (OLR), NAC, and EUSC are newly selected for this study.

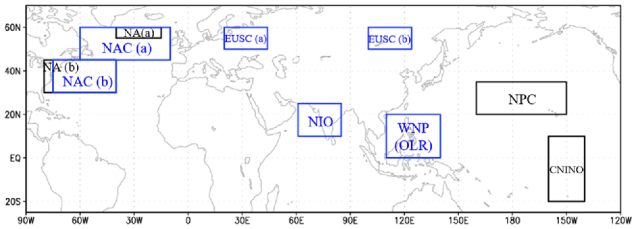

Fig. 2. Areas for the selected predictors. Black boxes represent areas of the three predictors selected by Lee and Seo (2013). Blue boxes represent areas of the additional four predictors selected in this study.

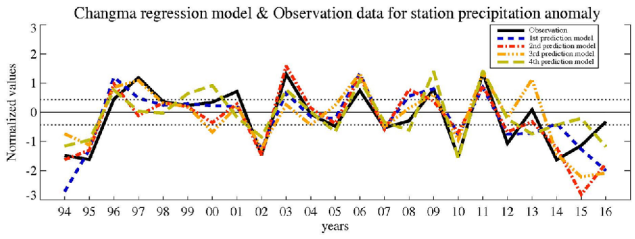

Fig. 3. Observed (black solid line) and predicted precipitation anomalies for each model (1st prediction model: blue dashed line, 2nd prediction model: red dashed-dot line, 3rd prediction model: orange dash-dot-dot-dot line, and 4th prediction model: yellow long-dash line). The dotted horizontal lines represent 0.43 and –0.43, respectively.

Table 2. Correlation coefficient, MSSS, and GMSS for the period from 1994 to 2016 for each prediction model and ensemble prediction model.

Forecast model	Correlation	MSSS	GMSS
1st prediction model	0.77	0.51	0.71
2nd prediction model	0.78	0.48	0.66
3rd prediction model	0.75	0.46	0.64
4th prediction model	0.77	0.58	0.52
Ensemble prediction model	0.82	0.66	0.83

To predict Changma rainfall intensity, four regression models are constructed using the forward stepwise regression method. As indicated in section 2b, the training period is 1994-2011 and the four multiple linear regression models for the last training set are:

$$\hat{Y} = +0.41[NA1] + 0.46[NPC] - 0.40[CNINO]$$

$$\hat{Y} = +0.57[NA1] + 0.33[NPC] - 0.41[WNP(OLR)]$$

$$\hat{Y} = +0.53[NA1] - 0.34[NIO] + 0.47[EUSC]$$

$$\hat{Y} = -0.39[NAC] + 0.47[NPC] - 0.50[CNINO],$$

where the dependent variable represents normalized Changma rainfall anomalies (Fig. 3, black line), and each independent variable on the right-hand side of the equations represents springtime predictors. The regression coefficients indicate the relative weighting among predictors. Here, the first regression model (1) is developed by Lee and Seo (2013). Observation (black line) and model predictions (blue, red, and orange dotted lines) are shown in the figure.

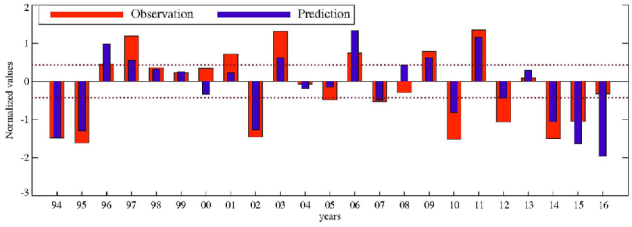

Fig. 4. Observed (red bars) and ensemble-mean predicted (blue bars) precipitation anomalies. The dotted horizontal lines represent 0.43 and –0.43, respectively.

Table 3. Contingency table for validation of the simple ensemble prediction. The abscissa shows the prediction results and the ordinate shows the observations. The above, normal, and below cases are divided by ± 0.43 after standardization. The percentage value of accurate prediction years to all years is about 87%.

		Prediction		
		Above	Normal	Below
Observation	Above	1996, 1997 2003, 2006, 2009, 2011	2001	
	Normal		1998, 1999, 2000, 2004, 2008, 2013	2016
	Below		2005	1994, 1995, 2002, 2005, 2010, 2012, 2014, 2015

Table 2 shows the prediction skill for Changma rainfall using the prediction models. The regression coefficients vary according to the training set. As these coefficients are fixed in 2011, the years since (2012 to 2016) are predicted with the same prediction model (as shown in the above equation). Correlation skill scores for the four prediction models are similar (0.75~0.78). However, MSSS (mean square-error skill score) and GMSS differ, with the former ranging from 0.46 to 0.58 and the latter from 0.52 to 0.71. To obtain a better prediction skill, we perform a simple arithmetic ensemble mean as shown by the blue bars in Fig. 4. The temporal correlation coefficient between observation and prediction is about 0.82 with an MSSS of about 0.66 and a GMSS as high as 0.83. The skill scores based on correlation, MSSS, and GMSS are improved by about 9%, 17%, and 19%, respectively, compared with those by Lee and Seo (2013). Table 3 is the contingency table showing the tercile prediction results (Wilks, 2006). The improvement occurs in the ensemble forecast, where the hit rate increases to 87.0% (cf., 73.9% in Lee and Seo, 2013).

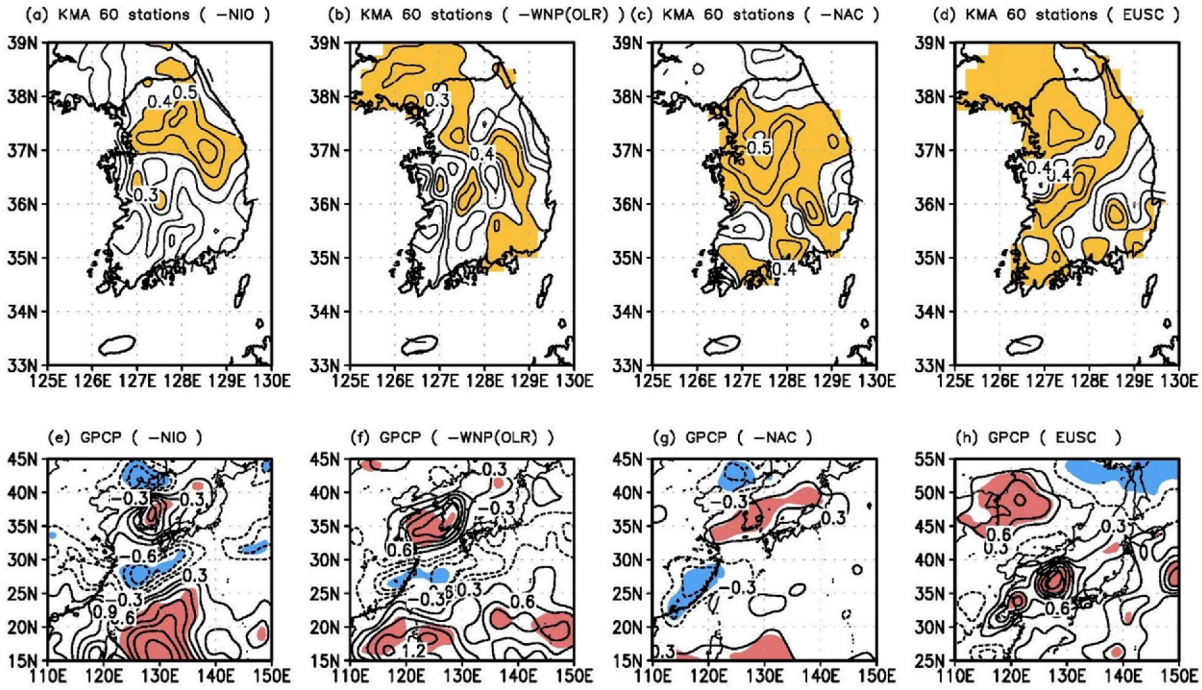

Fig. 5. Spatial correlation maps (contour intervals of 0.1) between the KMA's 60 station precipitation anomalies during 15 June to 31 July for the training period 1994-2011 and (a) the reversed NIO, (b) the reversed WNP (OLR), (c) the reversed NAC, and (d) the EUSC time series. The GPCP anomalies (contour intervals of 0.3 mm d^{-1}) regressed against (e) the reversed NIO, (f) the reversed WNP (OLR), (g) the reversed NAC, and (h) the EUSC time series from 15 June to 29 July for the period 1994-2011. Shading indicates statistically significant regions at the 90% confidence level.

4. Possible processes associated with predictors

In this section, we present the characteristics of the precipitation and circulation associated with the predictors during the Changma period (15 June-29 July) and discuss some possible processes. Figures 5a-d show spatial correlation maps between KMA's 60-station precipitation and each predictor; Figs. 5e-h show the regression patterns of GPCP precipitation anomalies with respect to individual predictor time series. Here, the signs of NIO, WNP (OLR), and NAC are reversed in order to demonstrate positive precipitation anomalies over the Korean peninsula. The significant correlations or signals in the plots represent an increase in precipitation over the Korean peninsula associated with these predictors (Fig. 5). Additionally, we can see that enhanced precipitation occurs following the southwest-to-northeastward elongated monsoon front (Figs. 5e-h). Along with this, dry conditions appear to the south (at 25°-30°N, Figs. 5e-g) with positive precipitation anomalies located over the South China Sea (SCS) and the WNP at 10°-20°N. These results indicate that all predictors have a crucial impact on Changma rainfall.

Now we examine the possible physical processes associated with these predictors. Figure 6 shows SSTAs (Figs. 6a and c) and low-level circulation anomalies (Figs. 6b and d) regressed against the reversed NIO time series. In relation to the reversed NIO, significant negative SSTAs are seen over the entire Indian Ocean basin and the tropical Central Pacific during springtime (Fig. 6a). Negative SSTAs over the northern IO persist through the Changma period with somewhat reduced amplitude (Fig. 6c). Also, negative SSTs appear over the WNP and the tropical Central Pacific. Figures 6b and d exhibit the development of cyclonic circulation anomalies over the SCS and WNP regions, possibly due to forcing by the negative SSTs over the NIO and WNP. The divergent flow along 10°N over these regions during these two periods is a more statistically peculiar feature (i.e., shading) than the higher-latitude part of the cyclonic circulation. This cyclonic circulation anomaly induces southeasterly moisture advection and thus an increase in Changma rainfall. These interpretations are consistent with previous findings related to the effects of El Niño and equatorial Kelvin waves (Yang et al., 2007; Xie et al., 2009; Ding et al., 2010), albeit with a reversed sign. That is, El Niño-induced tropical Indian Ocean warming persists into the spring and early summer and influences the circulation anomalies over the WNP (Yang et al., 2007; Xie et al., 2009; Wang et al., 2013), and Indian Ocean SST warming tends to induce the summer WNP anticyclone through an equatorial Kelvin wave. Lee et al. (2005) and Yun et al. (2008) also proposed that Indian Ocean warming could help maintain the subsidence in the WNP area.

Figure 7 shows the 850-hPa geopotential height anomaly pattern regressed onto the reversed WNP (OLR) index. In Fig. 7a, the cyclonic circulation is evident over the WNP, which is due to the Rossby wave response to enhanced convection over

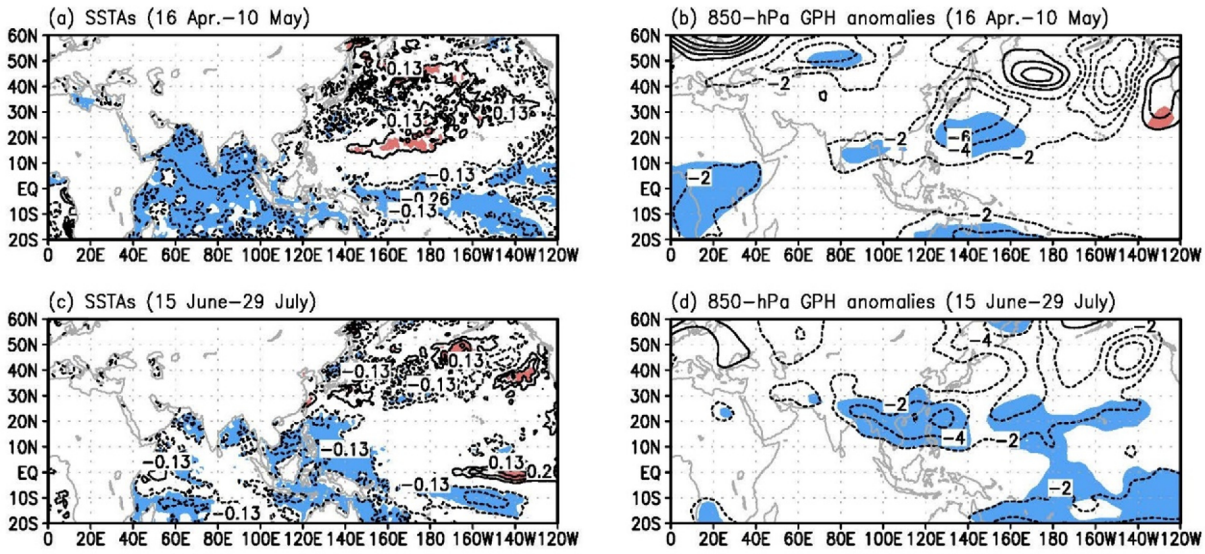

Fig. 6. Regressed SSTAs (contour intervals of 0.13 K) (a) from 16 April to 10 May and (c) from 15 June to 29 July, and regressed 850-hPa geopotential height anomalies (contour intervals of 2 m) (b) from 16 April to 10 May and (d) from 15 June to 29 July against the reversed NIO time series for 1994-2011. Shading indicates statistically significant regions at the 90% confidence level.

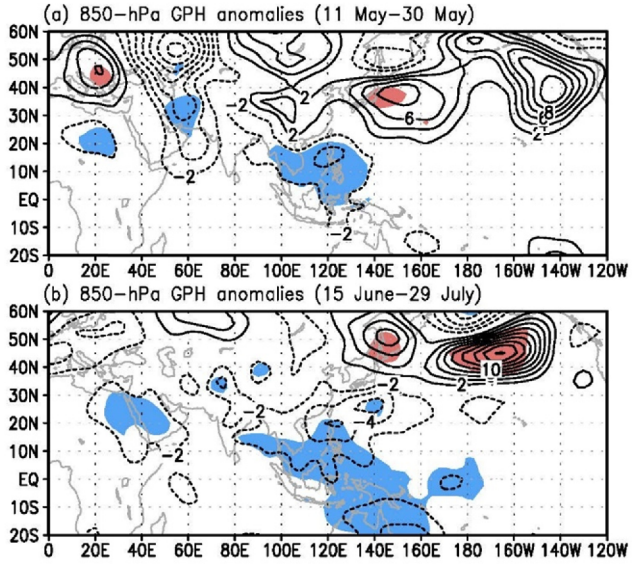

Fig. 7. Regressed (a) 850-hPa geopotential height anomalies (contour intervals of 2 m) from 11 May to 30 May, and (b) 850-hPa geopotential height anomalies from 15 June to 29 July against the reversed WNP (OLR) time series for 1994-2011. Shading indicates statistically significant regions at the 90% confidence level.

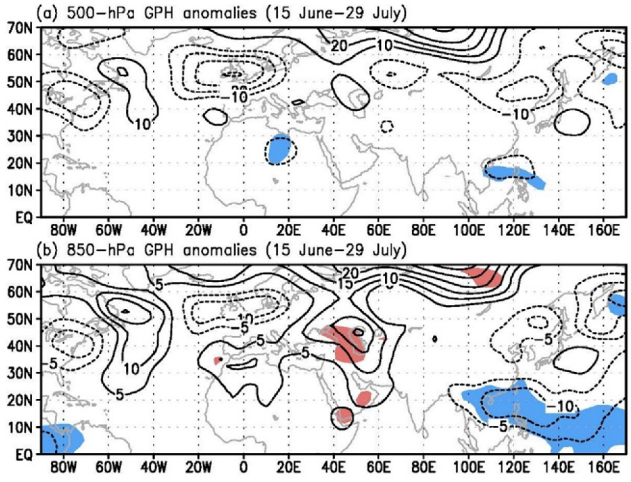

Fig. 8. Composite difference (strong minus weak) fields for (a) 500-hPa geopotential height anomaly (contour intervals of 10 m) and (b) 850-hPa geopotential height anomaly (contour intervals of 5 m) from 15 June to 29 July against the reversed NAC time series for 1994-2011. Composite criteria are ± 0.75. Shading indicates statistically significant regions at the 90% confidence level.

this region. The convective anomalies over the WNP may last until the Changma period due to a local SST feedback (Wang et al., 2000), leading to the maintenance of a persistent cyclonic circulation anomaly (Fig. 7b). The center of the cyclonic circulation slightly moves to the north and south-easterly or easterly wind anomalies bring about enhancement of Changma precipitation. Air-sea interaction processes may be involved in the sustainment of the circulation anomalies and northward expansion, but the details of these processes will require future investigation. Note that, similar to the NIO case, the formation of a cyclonic circulation anomaly to the south or southwest of the Korean peninsula is considered a major factor.

The North Atlantic change (NAC) is defined as the time difference (May-April) and domain difference in the North Atlantic region. The regressed pattern of SSTAs with respect to the reversed NAC index demonstrates a tripole pattern with two negative SSTA regions over the subpolar area (centered at 50°N) and subtropical region (centered at 30°N), and one

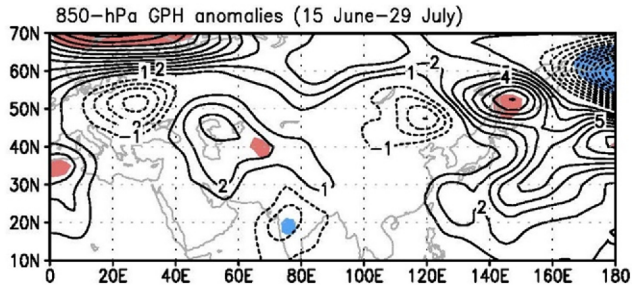

Fig. 9. Regressed (a) 850-hPa geopotential height anomalies (contour intervals of 1 m) from 15 June to 29 July against the EUSC time series for 1994-2011. Shading indicates statistically significant regions at the 90% confidence level.

positive SSTA region over the midlatitude western North Atlantic (centered at 38°N) (not shown). This tripolar structure is highly related to the positive phase of NAO and persists through the Changma period even if the anomaly amplitude becomes weak (not shown). Composite difference (strong minus weak) fields of 500- and 850-hPa geopotential height anomaly during the Changma period for the reversed NAC event are presented in Fig. 8. The variations of the North Atlantic SSTAs generate barotropic Rossby waves at the middle and lower troposphere, which propagate from the North Atlantic Ocean to East Asia (Fig. 8). The Rossby waves seem to propagate downstream in two branches with a higher latitude great-circle-like route affecting the anticyclonic circulation anomaly to the east of Japan and a lower-latitude branch inducing the cyclonic circulation anomaly over the SCS and WNP areas (even if the circulation anomaly is not seen over the Tibetan Plateau). These two circulation anomalies tend to induce southeasterly wind anomalies, which transport moisture to the Korean peninsula. It seems that the cyclonic circulation anomaly to the south is a more statistically significant feature. Previous studies (Wu et al., 2009; Seo et al., 2011; Lee and Seo, 2013; Park et al., 2015) also demonstrated the development of wave train-like teleconnection patterns over the Eurasian continent and East Asia during spring/summer.

To summarize, all three predictors (reversed NIO, reversed WNP (OLR), and reversed NAC) are associated with the generation or development of a cyclonic circulation anomaly to the south or southwest of the Korean peninsula, giving rise to moisture flux by southeasterly wind, which enhances Changma precipitation.

Figure 9 shows the 850-hPa geopotential height anomalies regressed onto the EUSC index. The two centers of the EUSC predictor are consistent with our expectation, where more snow cover leads to an in situ anticyclonic circulation anomaly (i.e., for the western box) and less snow cover results in a local cyclonic circulation anomaly (i.e., for the eastern box). However, it is of interest to see the significant anomaly over the Okhotsk Sea area (148°E, 50°N), which is a forced response to the EUSC dipole. The downstream circulation response tends to enhance the Okhotsk Sea high and thus confrontation with the NPSH air mass or the monsoon air mass located to the south. It is evident that the meridional gradient of equivalent potential temperature, which a good proxy for the front, is intensified (not shown). Therefore, this process strengthens the Changma front and enhanced precipitation occurs along the front, in particular over its northeastern side (i.e., 137°E, 41°N). A more interesting observation is that the NPSH to the south of the front is strengthened (although the statistical significance is rather weak) and that this NPSH intensification results in the development of an anticyclonic circulation anomaly to the south of the Korean peninsula, which additionally causes southwesterly flow of moisture toward the peninsula and enhances Changma rainfall. A more detailed process needs to be verified in future studies.

Previous studies indicate the appearance of a relationship between the Eurasian snow cover dipole and EASM precipitation (Yim et al., 2010). Matsumura et al. (2010, 2015) demonstrated that springtime Eurasian snow cover variability can alter land-atmosphere interaction by producing anomalous surface and atmospheric heating or cooling, which in turn influences northern atmospheric circulation including the summer Okhotsk Sea high. However, elucidation of the detailed mechanism is subject to further in-depth studies.

5. Analysis and verification of the recent Changma characteristics

In this section, we examine how the dominant predictors used in the prediction models affect Changma rainfall variations for the most recent three years. To do so, dates influenced by typhoon events are excluded. Figures 10a, c, and e shows the 850-hPa geopotential height anomaly fields during the Changma period for 2014, 2015, and 2016. The right panels (Figs. 10b, d, and f) exhibits the regressed fields of the 850-hPa geopotential height anomalies during the Changma period with respect to springtime predictors that influenced Changma rainfall for most for each year.

For 2014, the reversed NA1 appears to play a dominant role in the decrease of Changma rainfall. In relation to the significant precursor signal of the reversed NA1, the cyclonic circulation anomalies were expected to develop to the southeast of Japan as shown in Fig. 10b, and the observed geopotential height anomaly (Fig. 10a) also exhibits the cyclonic anomaly in a similar region. This pressure distribution gave rise to a decrease in Changma precipitation (Fig. 4). The ensemble forecast also predicted below-normal Changma precipitation (Fig. 4). For 2015, El Niño conditions are dominantly related to the change in Changma rainfall. Positive SSTA (i.e., positive CNINO signal) prevailed in the eastern and Central Pacific and, due to this forcing, anomalous cyclonic circulation to the east of Japan was enhanced along with anomalous anticyclonic circulation over the WNP and SCS (Fig. 10d). This configuration also appeared during the 2015 Changma period (Fig. 10c), albeit with a weaker

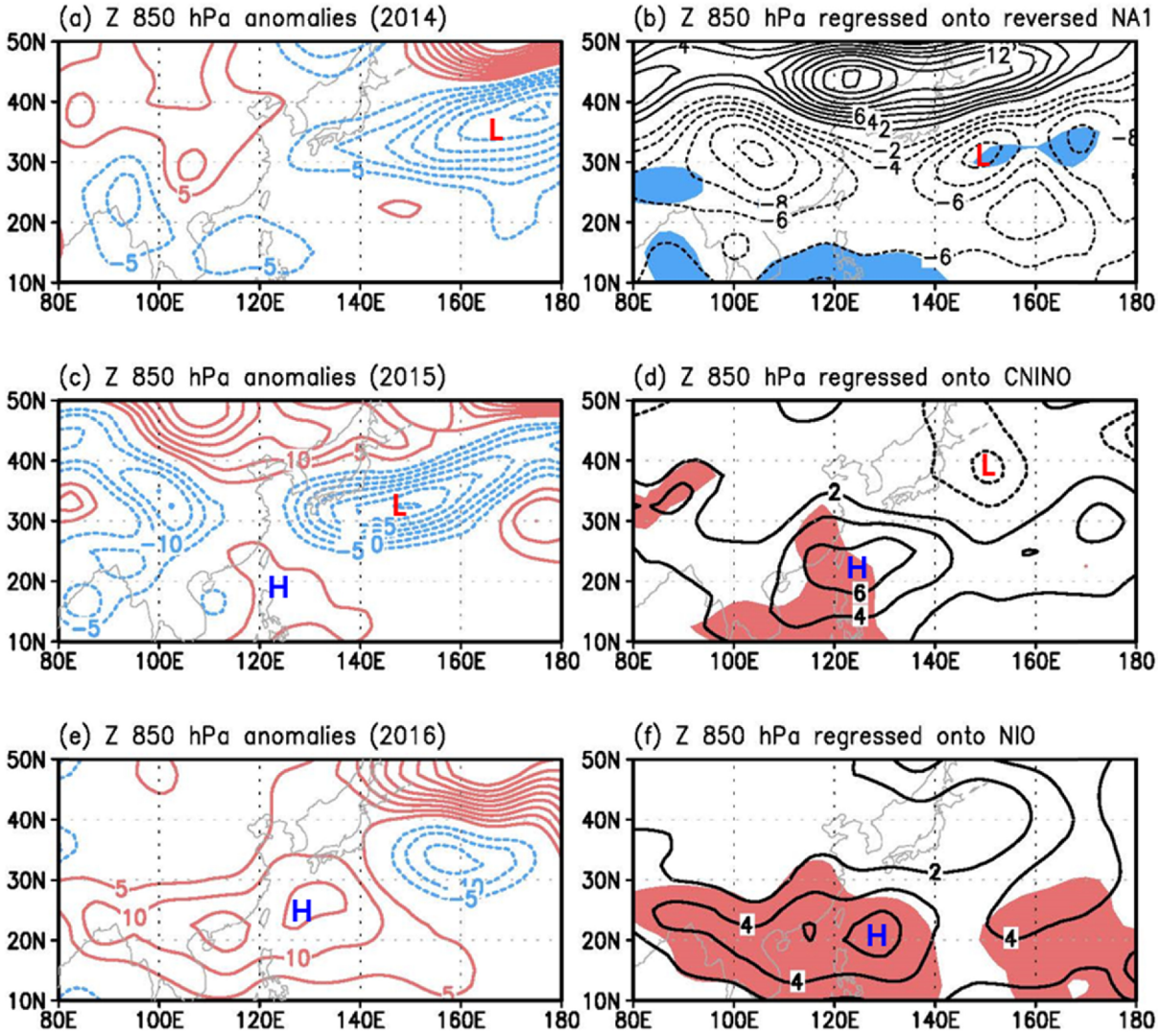

Fig. 10. Observed 850-hPa geopotential height anomalies (contour intervals of 5 or 10 m) from 15 June to 31 July for (a) 2014, (c) 2015, and (e) 2016. Regressed 850-hPa geopotential height anomalies (contour intervals of 2 m) from 15 June to 29 July against the reversed (b) NA1, (d) the CNINO, and (f) the NIO time series for 1994-2011. Shading indicates statistically significant regions at the 90% confidence level.

amplitude. Northerly winds were dominant, leading to a below-normal Changma precipitation year (Fig. 4).

Then, in 2016, positive SSTAs over the Central Pacific Ocean started to decay in spring. In contrast, over the northern Indian Ocean, positive SSTAs developed during spring and summer due to the well-known delayed effect of El Niño. Accordingly, a large projection onto the NIO is expected and the regressed low-level circulation feature is a strengthening in the WNP subtropical high with an enhanced easterly wind anomaly in the northern subtropics (10°-16°N) as shown in Fig. 10f. The observed circulation exhibited a similar feature (Fig. 10e). Since the large NIO precursor amplitude is projected to cause a decrease in Changma rainfall, a below-normal precipitation was predicted in the forecast scheme. For this year, however, the observed rainfall amount is recorded as near normal (Fig. 4). This is because a typhoon called Nepartak developed in the Philippine Sea during 1-5 July 2016, which pushed the small anticyclonic circulation anomaly to an area south of the Korean peninsula, resulting in an abrupt strengthening of the Changma front and heavy rainfall. About 78% of total Changma rainfall for this year has fallen during this short period. This very short transient effect is not represented even in the observed composite low-level circulation field as shown in Fig. 10e; therefore, in this case an incorrect tercile prediction based on the statistical forecast scheme is inevitable.

6. Summary

A one-month lead statistical forecast of Changma pre-

cipitation over South Korea has been performed in Lee and Seo (2013), where the three selected springtime predictors are SSTAs over the North Atlantic (NA1), the North Pacific (NPC), and the tropical Central Pacific (CNINO). Since a variety of precursor signals located upstream and downstream of the Korean peninsula impact the Changma precipitation, more prediction equations must be constructed to enhance prediction skills. To this end, we investigate additional potential predictors to create further prediction schemes.

Four additional predictors are found based on oceanic, land and atmospheric variables: NIO, WNP (OLR), NAC, and EUSC. Using these predictors, three additional prediction schemes are developed. A simple arithmetic ensemble mean produces much improved forecast skill compared to the original prediction model of Lee and Seo (2013). Skill scores measured by temporal correlation and MSSS are improved by about 9% and 17%, respectively. Both GMSS and hit rate based on a tercile prediction validation scheme are also enhanced by about 19% and 13%, respectively.

The three predictors (reversed NIO, reversed WNP (OLR), and reversed NAC) are all related to the development of a cyclonic circulation anomaly to the south or southwest of the Korean peninsula, which induces southeasterly moisture flux into the peninsula and increases Changma precipitation. The EUSC predictor acts to enhance the Okhotsk Sea high downstream, thus strengthening the Changma front. The latter also seems to induce a westward expansion of the NPSH and the ensuing development of an anticyclonic circulation anomaly to the south of the Korean peninsula, which further delivers southwesterly moist flow to the peninsula.

Thus, all these predictors (including the previously described three predictors) are related to the enhancement of anomalous circulation anomalies that produce a southerly type of wind. This takes place, in general, when either the center of the induced cyclonic circulation anomaly is located to the southwest of the Korean peninsula or that of the anticyclonic circulation anomaly is located to the south or southeast of the peninsula.

For the most recent three years, the reversed NA1 (for 2014), CNINO (for 2015), and NIO (for 2016) predictors all operate to induce a northerly type of wind during the Changma period over the Korean peninsula, which is consistent with the expectations mentioned above, resulting in a higher prediction skill for Changma rainfall.

The results of this study shed light on Changma precipitation forecasting, and the developed statistical schemes can be used as an aid for operational seasonal forecasting. However, the detailed dynamical processes including delayed influences in relation to the predictors discussed in this paper, need to be investigated by a more in-depth analysis and various sensitivity tests using a simple linear baroclinic model, general circulation model, and atmosphere-ocean coupled model.

Acknowledgements. This work was funded by the Korea Meteorological Administration Research and Development Program under Grant KMIPA 2015-2113. The authors would like to acknowledge the support from the Korea Institute of Science and Technology Information (KISTI). We are grateful to the editor and two anonymous reviewers for their helpful and constructive comments.

Edited by: Akio Kitoh

References

Adler, R. F., and Coauthors, 2003: The version 2 Global Precipitation Climatology Project (GPCP) monthly precipitation analysis (1979 - present). *J. Hydrometeor.*, **4**, 1147-1167, doi:10.1175/1525-7541(2003)004<1147:TVGPCP>2.0.CO;2.

Blockeel, H., and J. Struyf, 2002: Efficient algorithms for decision tree cross-validation. *J. Mach. Learning Res.*, **3**, 621-650, doi:10.1162/jmlr.2003.3.4-5.21.

Chen, X., and T. Zhou, 2014: Relative role of tropical SST forcing in the 1990s periodicity change of the Pacific-Japan pattern interannual variability. *J. Geophys. Res.*, **119**, 13043-13066, doi:10.1002/2014JD-022064.

Chu, J.-E., S. N. Hameed, and K.-J. Ha, 2012: Non-linear, intraseasonal phases of the East Asian summer monsoon: Extraction and analysis using self-organizing maps. *J. Climate*, **25**, 6975-6988, doi:10.1175/JCLI-D-11-00512.1.

Ding, R. Q., K.-J. Ha, and J. P. Li, 2010: Interdecadal shift in the relationship between the East Asian summer monsoon and the tropical Indian Ocean. *Climate Dyn.*, **34**, 1059-1071, doi:10.1007/s00382-009-0555-2.

Kanamitsu, M., W. Ebisuzaki, J. Woollen, S. K. Yang, J. J. Hnilo, M. Fiorino, and G. L. Potter, 2002: NCEP-DOE AMIP-II Reanalysis (R-2). *Bull. Amer. Meteor. Soc.*, **83**, 1631-1643, doi:10.1175/BAMS-83-11-1631.

Kim, J.-Y., and K.-H. Seo, 2014: The development of Ensemble Statistical Prediction Model for Changma precipitation. *Korean Meteor. Soc.*, **24**, 533-540, doi:10.14191/Atmos.2014.24.4.533 (in Korean with English abstract).

Kwon, M., J.-G. Jhun, B. Wang, S.-I. An, and J.-S. Kug, 2005: Decadal change in relationship between east Asian and WNP summer monsoons. *Geophys. Res. Lett.*, **32**, L16709, doi:10.1029/2005GL023026.

Lee, E.-J., J.-G. Jhun, and C.-K. Park, 2005: Remote connection of the northeast Asian summer rainfall variation revealed by a newly defined monsoon index. *J. Climate*, **18**, 4381-4393, doi:10.1175/JCLI3545.1.

Lee, S.-E., and K.-H. Seo, 2013: The development of a statistical forecast model for Changma. *Wea. Forecasting*, **28**, 1304-1321, doi:10.1175/WAF-D-13-00003.1.

Lee, S.-S., J.-Y. Lee, K.-J. Ha, B. Wang, and J. Schemm, 2011: Deficiencies and possibilities for long-lead coupled climate prediction of the western North Pacific-East Asian summer monsoon. *Climate Dyn.*, **36**, 1173-1188, doi:10.1007/s00382-010-0832-0.

Matsumura, S., K. Yamazaki, and T. Tokioka, 2010: Summertime land atmosphere interactions in response to anomalous springtime snow cover in northern Eurasia. *J. Geophys. Res.*, **115**, D20107, doi:10.1029/2009JD012342.

_____, _____, and T. Sato, 2015: Role of Siberian land atmosphere coupling in the development of the August Okhotsk High in 2008. *J. Meteor. Soc. Japan*, **93**, 229-244, doi:10.2151/jmsj.2015-013.

Oh, H., and K.-J. Ha, 2016: Prediction of dominant intraseasonal modes in the East Asian-western North Pacific summer monsoon. *Climate Dyn.*, **47**, 2025-2037, doi:10.1007/s00382-015-2948-8.

Park, H.-L., K.-H. Seo, and J.-H. Son, 2015: Development of a Dynamics-Based Statistical Prediction Model for the Changma Onset. *J. Climate*,

28, 6647-6666, doi:10.1175/JCLI-D-14-00502.1.

Reynolds, R. W., T. M. Smith, C. Liu, D. B. Chelton, K. S. Casey, and M. G. Schlax, 2007: Daily high-resolution-blended analyses for sea surface temperature. *J. Climate*, **20**, 5473-5496, doi:10.1175/2007JCLI1824.1.

Robinson, D. A., K. F. Dewey, and R. R. Heim, 1993: Global snow cover monitoring: An update. *Bull. Amer. Meteor. Soc.* **74**, 1689-1696, doi:10.1175/1520-0477(1993)074<1689:GSCMAU>2.0.CO;2.

Seo, K.-H., J.-H. Son, and J.-Y. Lee, 2011: A new look at Changma. *Korean Meteor. Soc.*, **21**, 109-121 (in Korean with English abstract).

_____, _____, _____, and H.-S. Park, 2015: Northern East Asian monsoon precipitation revealed by air mass variability and its prediction. *J. Climate*, **28**, 6221-6233, doi:10.1175/JCLI-D-14-00526.1.

Wang, B., R. Wu, and X. Fu, 2000: Pacific-East Asian teleconnection: How does ENSO affect East Asian Climate? *J. Climate*, **13**, 1517-1536, doi:10.1175/1520-0442(2000)013<1517:PEATHD>2.0.CO;2.

_____, J.-G. Jhun, and B.-K. Moon, 2007: Variability and singularity of Seoul, South Korea, rainy season (1778-2004). *J. Climate*, **20**, 2572-2580, doi:10.1175/JCLI4123.1.

_____, B. Xiang, and J.-Y. Lee, 2013: Subtropical high predictability establishes a promising way for monsoon and tropical storm predictions. *Proc. Natl. Acad. Sci. USA*, **110**, 2718-2722, doi:10.1073/pnas.1214626110.

Wilks, D. S., 2006: *Statistical Methods in the Atmospheric Sciences*. 2nd ed. Academic Press, 630 pp.

Wu, Z., B. Wang, J. Li, and F.-F. Jin, 2009: An empirical seasonal prediction model of the east Asian summer monsoon using ENSO and NAO. *J. Geophys. Res.*, **114**, D18120, doi:10.1029/2009JD011733.

Xie, S.-P., K. Hu, J. Hafner, H. Tokinaga, Y. Du, G. Huang, and T. Sampe, 2009: Indian Ocean capacitor effect on Indo- western Pacific climate during the summer following El Niño. *J. Climate*, **22**, 730-747, doi:10.1175/2008JCLI2544.1.

Yang, J., Q. Liu, S.-P. Xie, Z. Liu, and L. Wu, 2007: Impact of the Indian Ocean SST basin mode on the Asian summer monsoon. *Geophys. Res. Lett.*, **34**, L02708, doi:10.1029/2006GL028571.

Yim, S.-Y., J.-G. Jhun, R. Lu, and B. Wang, 2010: Two distinct patterns of spring Eurasian snow cover anomaly and their impacts on the East Asian summer monsoon. *J. Geophys. Res.*, **115**, D22113, doi:10.1029/2010JD013996.

_____, B. Wang, and W. Xing, 2014: Prediction of early summer rainfall over South China by a physical-empirical model. *Climate Dyn*., **43**, 1883-1891, doi:10.1007/s00382-013-2014-3.

_____, _____, and _____, 2015: Peak-summer East Asian rainfall predictability and prediction part II: Extratropical East Asia. *Climate Dyn.*, **47**, 15-30, doi:10.1007/s00382-015-2849-x.

Yun, K.-S., K.-H. Seo, and K.-J. Ha, 2008: Relationship between ENSO and northward propagating ISO in the East Asian summer monsoon system. *J. Geophys. Res.*, **113**, D14120, doi:10.1029/2008JD009901.